Optimized numerical solutions of SIRDVW multiage model for the vaccination roll-out during the third pandemic wave of SARS-CoV-2: the Italian case study. Supporting Information.

S1. Parameters Setting for the Italian scenario

In Section 3, the parameters involved in the model have been set as follows:

- $I = (0, T_f]$, $T_f = 151$ (days): the epidemiological model is set in Italy on the period ranging from January 1$^{\text{st}}$, 2021 to June 1$^{\text{st}}$, 2021 (*i.e.* the six-month period that starts with the beginning of the vaccination campaign and concurrent with the third pandemic wave).

- $\beta \in (0, 1)$: transmission rate, depending on the implemented Non-Pharmaceutical Interventions (NPIs) and virus transmissibility. It is assumed to be constant across all ages as in [1];

- $\sigma_V, \sigma_W \in (0, 1)$: vaccine effectiveness on transmissibility after administration of first dose (the former) or completing the cycle (the latter). It can be interpreted as the ratio of transmissibility between vaccinated individuals and unvaccinated ones. The value 0 means that the vaccine is fully effective, 1 totally ineffective;

- $\theta_V, \theta_W \in (0, 1)$: vaccine effect on mortality after administration of first dose (the former) or completing the cycle (the latter). It can be interpreted as the ratio of probability of getting severe symptoms between vaccinated individuals and unvaccinated ones. The value 0 means that the vaccine is fully effective, 1 totally ineffective;

- IFR_i: age-dependant Infection Fatality Rate estimated starting from available data from Dipartimento di Protezione Civile Italiana as in [2];

- In the fatality function $f_i(S_i, V_i, W_i)$ the amount of days after the inoculation that we consider for reaching the complete vaccine effectiveness t_a is fixed at 15 days;

- C_{ik}: i, k-th entry of the contact matrix, tracing back contacts between ages starting from the POLYMOD surveys [3] (see Figure ST1);

- r_i: susceptibilities to infection depending on age, drawn from [4], previously adopted by [1];

- γ: recovery rate from the disease infection, which is maintained constant across ages. Since infectious individuals are supposed to exit from the correspondent compartment with flux γI_i, the parameter γ is interpreted as the inverse of the average time of recovery t_R. The distribution of recovery times is treated as a Gaussian distribution with mean $\bar{t}_R = 14.20$ (days) and variance $\sigma^2 = 5.94$ (days^2) as in [5]. We actually draw the posterior distribution of the parameter γ from the calibration stage (see S2 for more details);

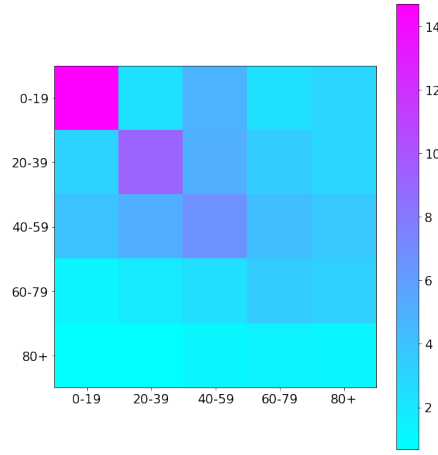- N_i: Number of individuals in the i-th age stratification;

Figure ST1: Contact matrix retrieved by [3] for the specific age-classes contemplated in the model.

- μ_R: natural waning immunity rate, taking into account plausible reinfections coming from previously-recovered individuals. This parameter has not shown peculiar dependence on age and has been retrieved from [6, 7];

- $I_{u,i}(t) = (1 - \delta(t))I_i(t)$ $t \in$ I: approximate number of undetected individuals whose age falls in the i-th stratification at time t. As in [8], we compute the detection rate δ from the ratio of the computed Case Fatality Ratio (CFR) and the theoretical Infectious Fatality Ratio (IFR) for COVID19 independently on ages;

- δ_w: elapsing time among subsequent administrations to be chosen in the admissible set $\{21, 28, 35, 42\}$ days. In the Italian scenarios, it has been set at 21 days;

- $U_{1,i}$, $U_{2,i}$, $U_{R,i}$: daily amount of administered first doses, second doses and doses administered to the i-th age-class, respectively. The choice of these variables is coherent with actual implementation of the Italian vaccination campaign: two consecutive doses to be administered for completing the vaccination cycle to Susceptible individuals, one single administration to Recovered ones. To reduce the computational complexity of the model we assume that the functions $U_{1,i}(t)$, $U_{2,i}(t)$, $U_{R,i}(t)$ are piecewise constant (constant on each week) and the weekly value of administrations is supposed to be equally distributed among each day of the week. In Figure ST2 we present the history of the daily administrations in Italy during the period of interest, while in Figure ST3 the corresponding averages over the weeks are reported.

Remark. During the Italian vaccination campaign, the mRNA-based vaccines Pfizer/BioNTech Comirnaty (BNT162b2) and SpikeVax (previously COVID-19 Moderna mRNA–1273) have been administered more extensively. The values of the parameters σ and θ reported in Table SF1 have been deduced assuming to deal with a Pfizer/BioNTech kind of vaccine. The effectiveness of the vaccine on reducing both transmissibility and severity of symptoms has been previously assessed through medical trials (see *e.g.* [9]) and then posteriorly confirmed through the available epidemic data [10]. However, given the potential relevant impact of σ and θ on the optimality of the vaccination campaign, in S3 we carry out a sensitivity analysis of these parameters.
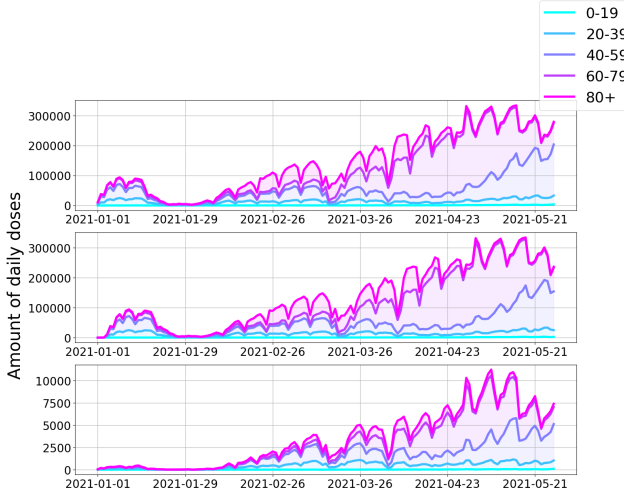
2

Figure ST2: Amount of first doses, second doses and doses administered to recovered during the time frame of interest retrieved from DPC data [11].
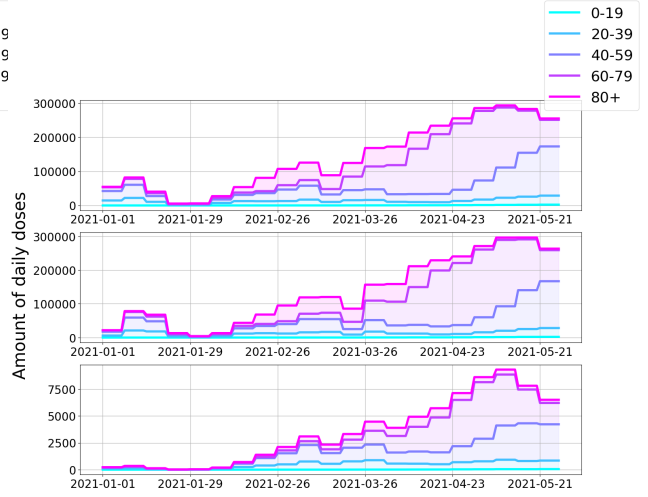

Figure ST3: Amount of first doses, second doses and doses administered to recovered during the time frame of interest retrieved from DPC data [11], and then averaged per weeks.

Parameter	(0,19)	(20,39)	(40,59)	(60,79)	(80+)	Reference
γ	\multicolumn{5}{c}{0.07}	[5]
r_i	0.33	1	1	1	1.47	[4]
IFR_i	1e-4	6e-4	4.5e-3	2.3e-2	7.2e-2	[2]
μ_R	\multicolumn{5}{c}{0.006}	[6, 7]
σ_V	\multicolumn{5}{c}{0.21}	[1]
σ_W	\multicolumn{5}{c}{0.21}	[1]
θ_V	\multicolumn{5}{c}{0.20}	[1]
θ_W	\multicolumn{5}{c}{0.037}	[1]

Table SF1: Table of the parameters adopted during the calibration stage.

The differential model has been endowed with proper initial conditions for each of the considered age-state compartment. The amount of initial deceased is deterministically fixed and it is retrieved by available data in [12]. On the other hand, we introduce uncertainty on the initial conditions for the Susceptible, Infectious and Recovered classes. This choice is dictated by a different level of accuracy of the available data for the different compartments. Finally, vaccinated individuals belonging to V and W compartments have been set to zero since our period of interest ranges from January 1$^{\text{st}}$, 2021 to June 1$^{\text{st}}$, 2021 (i.e. the six-month period coinciding with the beginning of the vaccination campaign and therefore with the third pandemic wave). Hence, we assume

$$
\begin{aligned}
I_i(0) &= \zeta_{I,i} I_{D,i,0} \\
R_i(0) &= \zeta_{R,i} R_{D,i,0} \\
S_i(0) &= \left(N_i - \left(I_i(0) + R_i(0) + D_i(0)\right)\right) \zeta_{S,i}
\end{aligned} \tag{1}
$$

where $X_{D,i}$ is the value of the X-th compartment retrieved from the Italian DPC data on January 1$^{\text{st}}$, 2021 and $\zeta_{X,i}$ are independent and identical uniform distributions in [0.7, 1.3]. The choice in (1) allows to introduce prior uncertainty to be posteriorly reconstructed after the Monte Carlo Markov Chain stage of the calibration process (see S2).

3

68 S2. Calibration process

69 Following [8], we undergo a double-stage calibration for the transmission rate β. The transmission rate

70 embodies the effects of non-pharmaceutical interventions due to the Italian government's political decisions,

71 updated on a weekly basis during the period of concern. Hence, the parameter is assumed to be piecewise-

72 constant over one-week-long intervals (*time-phases* in the sequel). Similarly, e.g., to [1]), we assume that

73 the transmission rate is independent of the age. In view of the above assumptions, we need to calibrate

74 21 parameters representing the values of the transmission rate β in each time-phase. Generally speaking,

75 calibration problems can be interpreted as deterministic inverse optimal control problems [13, 14, 15, 16], or

76 can be tackled through stochastic techniques [17, 18, 19]. Alternatively, calibration problems can be solved

77 by resorting to Machine-Learning based schemes (see *e.g.* [20, 21] and [22, 21, 23, 24]). In this paper the

78 calibration step is implemented by employing a classical two-stage process: (1) a Least Square (LS) phase is

79 used for retrieving acceptable estimators of the parameters; (2) every output of the LS phase is then adopted

80 as mean value for the corresponding prior distribution imposed during the classical Monte Carlo Markov Chain

81 (MCMC) approach (we refer to [25] for more details). For what concerns the calibration of the initial conditions

82 (1), we impose uniform priors on the initial values of S, I, R variables, while a Gaussian prior is employed for

83 the calibration of the recovery time variable $t_R = \frac{1}{\gamma}$. During both LS and MCMC stages of the calibration,

84 we minimize the adherence, for each age class i, of the deceased compartment D_i to the public available data

85 $D_{D,i}$:

$$\mathcal{E} = \sum_{i=0}^{N_{ages}} \int_0^{T_f} (D_i(t) - D_{D,i}(t))^2 \, dt. \tag{2}$$

86 In Figure ST5 the results of the calibration are shown. In particular, Figure ST5(a) represents the total

87 amount of deceased during the first six months of 2021 (dashed line) and the behavior of the median value

88 after the MCMC calibration, together with the credible interval of order 95% (shaded area). In Figure ST5(b)

89 we present the age repartition of deceased among age-classes. More precisely, the orange curve stands for the

90 amount of deceased after the LS-calibration, the red one for the median of the posterior, the black dashed

91 line represents the DPC data of deceased, while the shaded areas represents the 95% credible intervals for

92 each age-class. Notice that, as the cumulative number of recorded deceased cannot decrease, the decreasing

93 behaviour in Figure ST5(b) of the dashed line is probably due to reporting errors. The median trend of the

94 total amount of deceased is in agreement with the actual trend of the detected deaths recorded by the DPC;

95 the same variable lies in the 95% credible interval posteriorly recovered, as showed in Figure ST5(b). Moreover,

96 notice that the percentage repartition of deaths attained by the model with the calibrated transmission rate

97 agrees qualitatively with the age-repartition of deceased actually observed in Italy during the same period (see

98 Figure ST5(c)). To further assess the reliability of the output of the calibration process, the calibrated model

99 has also been validated by comparing the simulated amount of infected individuals with the corresponding data

100 value. In particular, in Figure ST6 the simulated detected infected individuals, computed as $I_{d,i}(t) = \delta I_i(t)$,

101 δ being the detection rate, are compared with the actual positive individuals recorded by [12]. As the the

102   number of infected individuals are not included in (2), the results of Figure ST6 show that the performance of

103   the implemented model with the calibrated parameter can be considered fully satisfactory. In this respect, we

104   also note that Figure ST6(b) shows an excellent accordance, in terms of age-percentage repartition of infected,

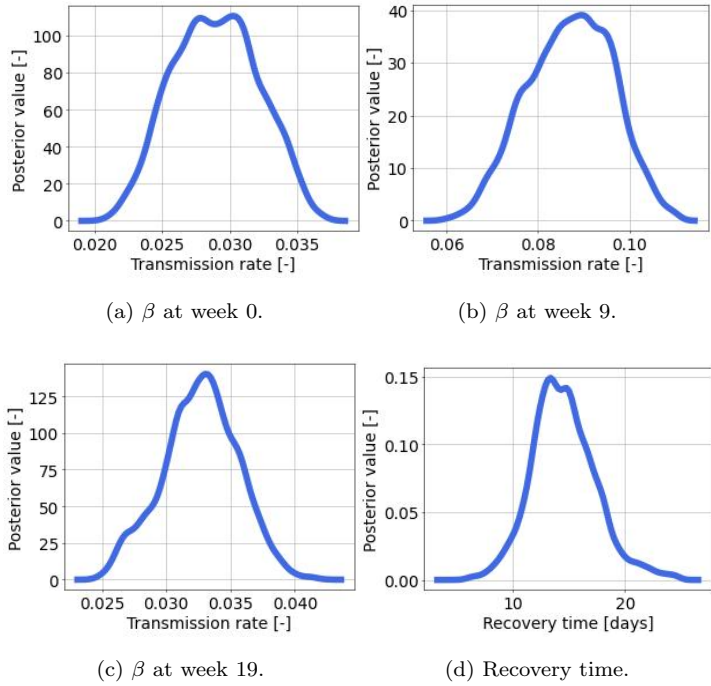105   between the public available data and the output of our calibrated model.

106

(a) β at week 0.

(b) β at week 9.

(c) β at week 19.

(d) Recovery time.

Figure ST4: Posterior distribution of three different transmission rates at the first (a), 9th (b) and 19th (c) week from the beginning of the simulation. (d) Posterior distribution of the recovery time variable.

| Week	β median value
1	0.02866168
2	0.08487043
3	0.05793916
4	0.03441935
5	0.04757512
6	0.07276475
7	0.08298755
8	0.07913101
9	0.07514123
10	0.07197278
11	0.07040295
12	0.06946485
13	0.06860226
14	0.06789474
15	0.06733712
16	0.06685438
17	0.06643925
18	0.0661041
19	0.03511503
20	0.02103584
21	0.01821423

Table SF2: Median values retrieved by the posterior distributions during each week of the calibration interval.
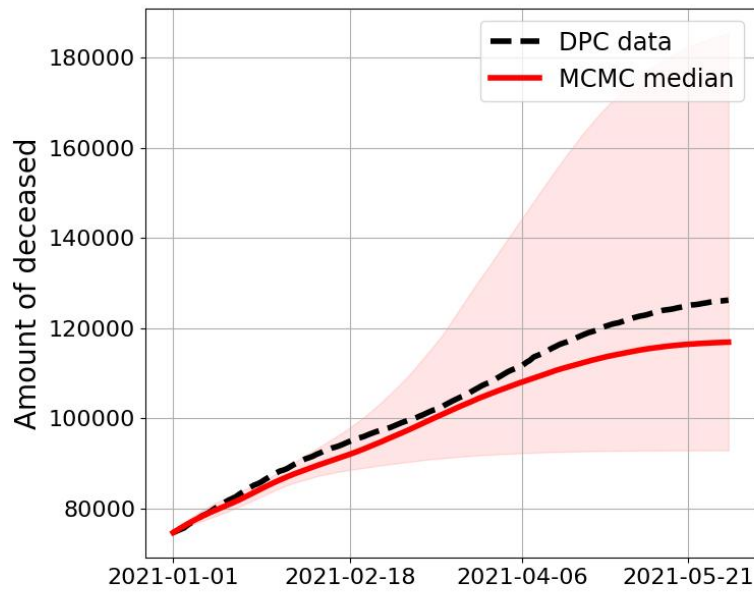
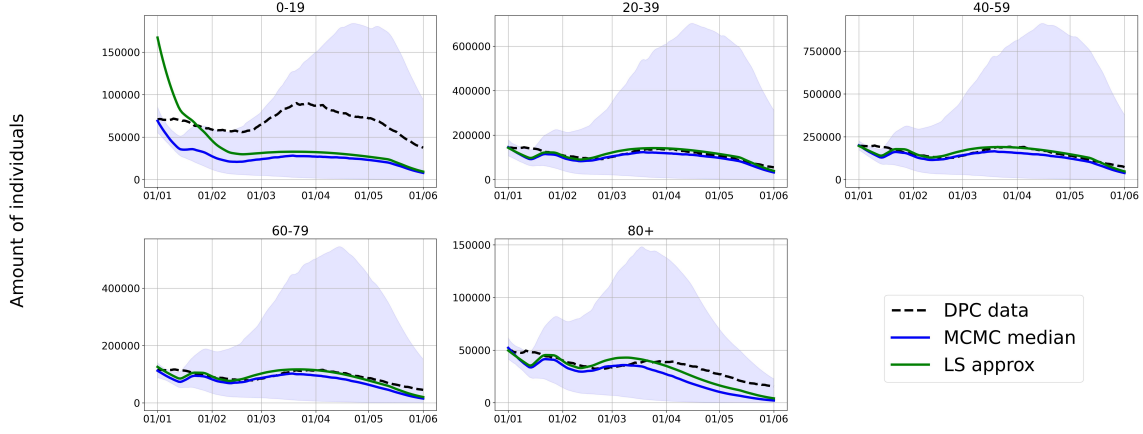(a) Total deceased after the calibration stages compared with the DPC data function.
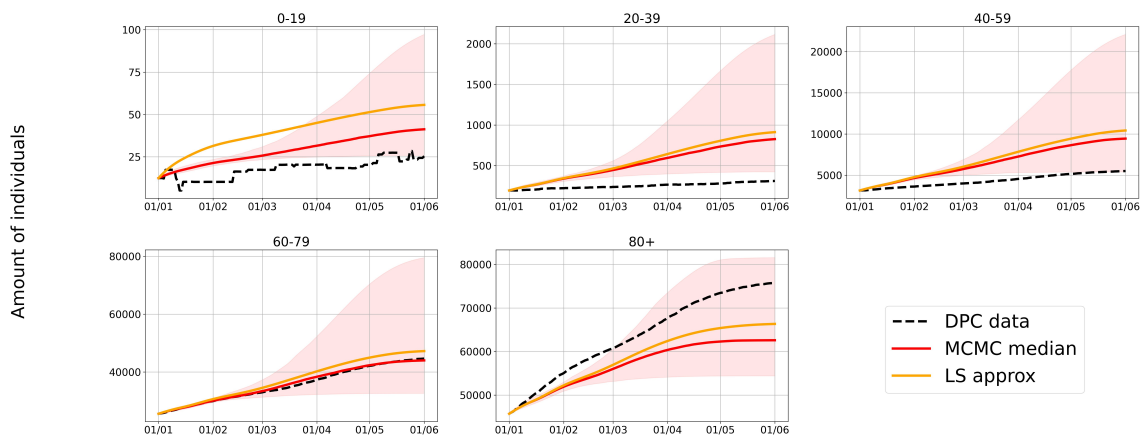
(b) Age-dependent evolution of deceased after the calibration stages compared with the DPC data [12] function.
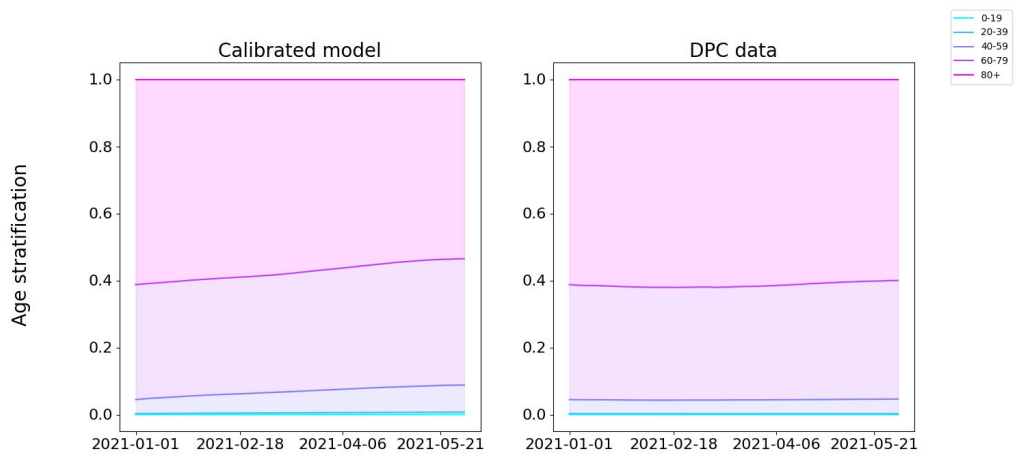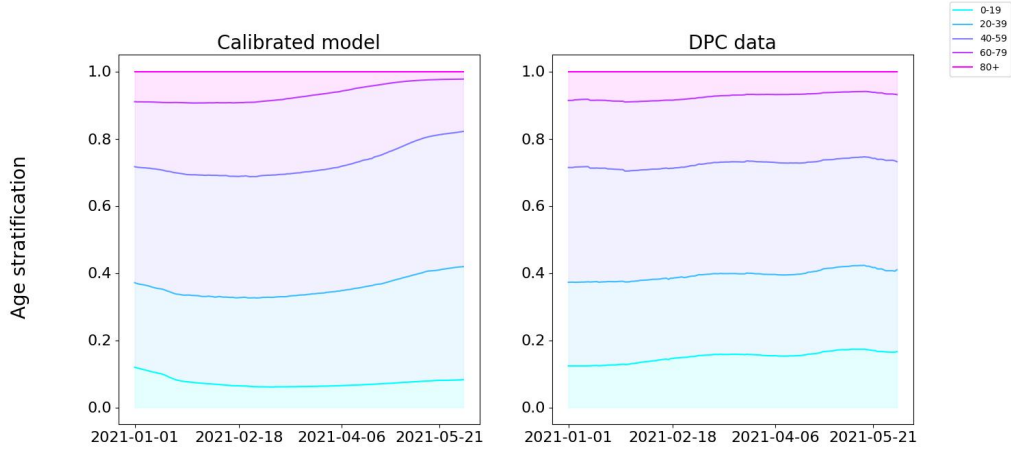

(c) Age-percentage repartition of deceased after the calibration stages compared with the DPC data [12] function.

Figure ST5: Deceased evolutions after the calibration.

(a) Age-dependent evolution of detected infected after the calibration stages compared with the DPC data [12] function.

(b) Age-percentage repartition of deceased after the calibration stages compared with the DPC data [12] function.

Figure ST6: Infected evolutions after the calibration.

S3. Sensitivity analyses

In this section we show the results of a sensitivity analysis of the reproduction number $\mathcal{R}_t$ with respect to the vaccination parameters $\theta_V, \theta_W, \sigma_V, \sigma_W$. The reproduction number of the model, measuring the amount of secondary cases infected by a primal one in a fully susceptible population, has been recovered following the Next Generation Matrix approach [26], *i.e.* by computing the spectral radius of the so-called next generation matrix associated to the model. In the following, we consider two different scenarios:

- **Scenario 1 (Figure ST7)**: Consider the dependency of $\mathcal{R}_t$ on the effectiveness in reducing transmissibility, covering the space of admissible parameters $\sigma_V, \sigma_W \in [0,1]$.

- **Scenario 2 (Figure ST8)**: Consider the dependency of $\mathcal{R}_t$ on the effectiveness in reducing severe infections, covering the space of admissible parameters $\theta_V, \theta_W \in [0,1]$.

It is well-known that the value of the reproduction number plays a key-role in the dynamics of the epidemic.

118 Indeed, it can be interpreted as a bifurcation parameter assessing whether an outbreak is starting or if the

119 epidemic is slowing down (threshold value for $\mathcal{R}_t$ is 1). In all the simulations, the value of the transmission rate

120 in each time phase is set equal to the median value obtained by the calibration process, while the recovery time

121 has been chosen equal to the median value of the posterior distribution of the MCMC calibration, *i.e.* 14.20

122 days. From Figures ST7(a) and ST8(a) we deduce that there is no evidence of the impact of the vaccination

123 parameters on the initial Reproduction number (also known as $\mathcal{R}_0$). Moreover, from Figure ST8 we observe

124 that variations of the severity reduction parameters θ_V, θ_W have very little impact (order 1e-9/1e-10) on the

125 reproduction number at different weeks. This is not unexpected since these parameters enter in the model

126 only through the fatality-function, thus impacting only the compartments R and D. More precisely, as the

127 reproduction number takes into account the amount of new infections and the infections cannot come from D

128 and R compartments (μ_R is a very slow rate), θ_V, θ_W are not relevant in the computation of $\mathcal{R}_t$. On the other

129 hand, the results reported in Figure ST7 show that the variations in the effectiveness of the vaccine (parameters

130 σ_V and σ_W) have relevant impact (order 1e-2) on reducing the transmissibility after the 8th week of simulation,

131 as a result of the increase in the amount of administrations. Looking at the slopes of the isolines in Figure ST7

132 we observe as the influence of σ_V becomes more prominent over the one of σ_W starting from week 10. Finally,

133 a close inspection of the isolines in the neighbourhoods of the values retrieved by medical analyses (red dots

134 in Figures ST7 and ST8) reveals that fixing deterministically the values of the vaccination parameters, rather

135 than dealing with its uncertainty, does not have a significant influence on the reproduction number.

(a) Week 0.

(b) Week 4.

(c) Week 8.

(d) Week 12.
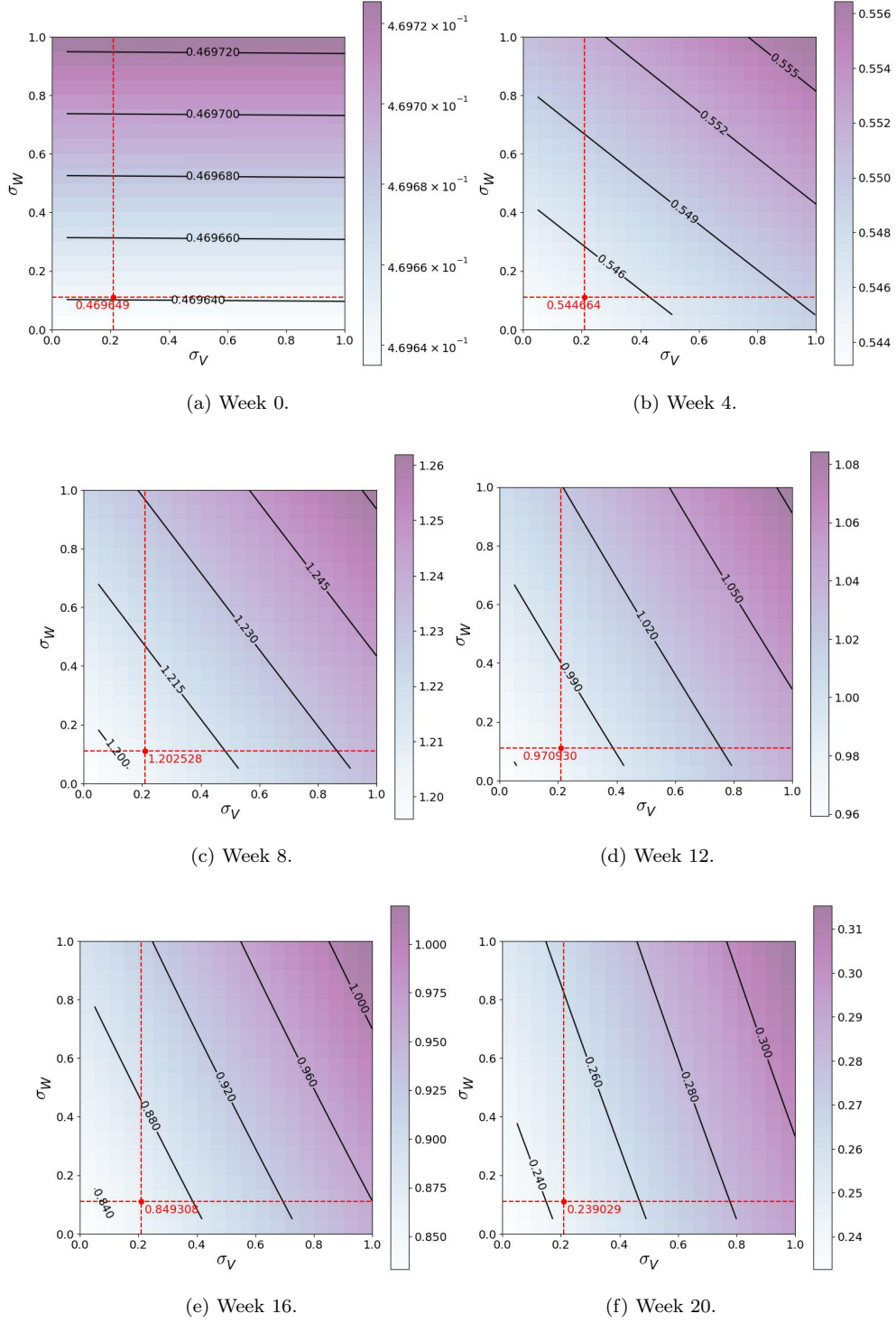
(e) Week 16.

(f) Week 20.

Figure ST7: Reproduction number at different weeks depending on the value assigned to the effectivenesses of doses on transmissibility. X-axis represents σ_V and Y-axis represents σ_W. The red point corresponds to the reference value, $i.e.$ $\mathcal{R}_t$ value with σ_V, σ_W as in Table SF1.

(a) Week 0.

(b) Week 4. Reference $\mathcal{R}_t = 0.54480551917$.

(c) Week 8. Reference $\mathcal{R}_t = 1.20322965963$.

(d) Week 12. Reference $\mathcal{R}_t = 0.97225228190$.

(e) Week 16. Reference $\mathcal{R}_t = 0.85123543297$.
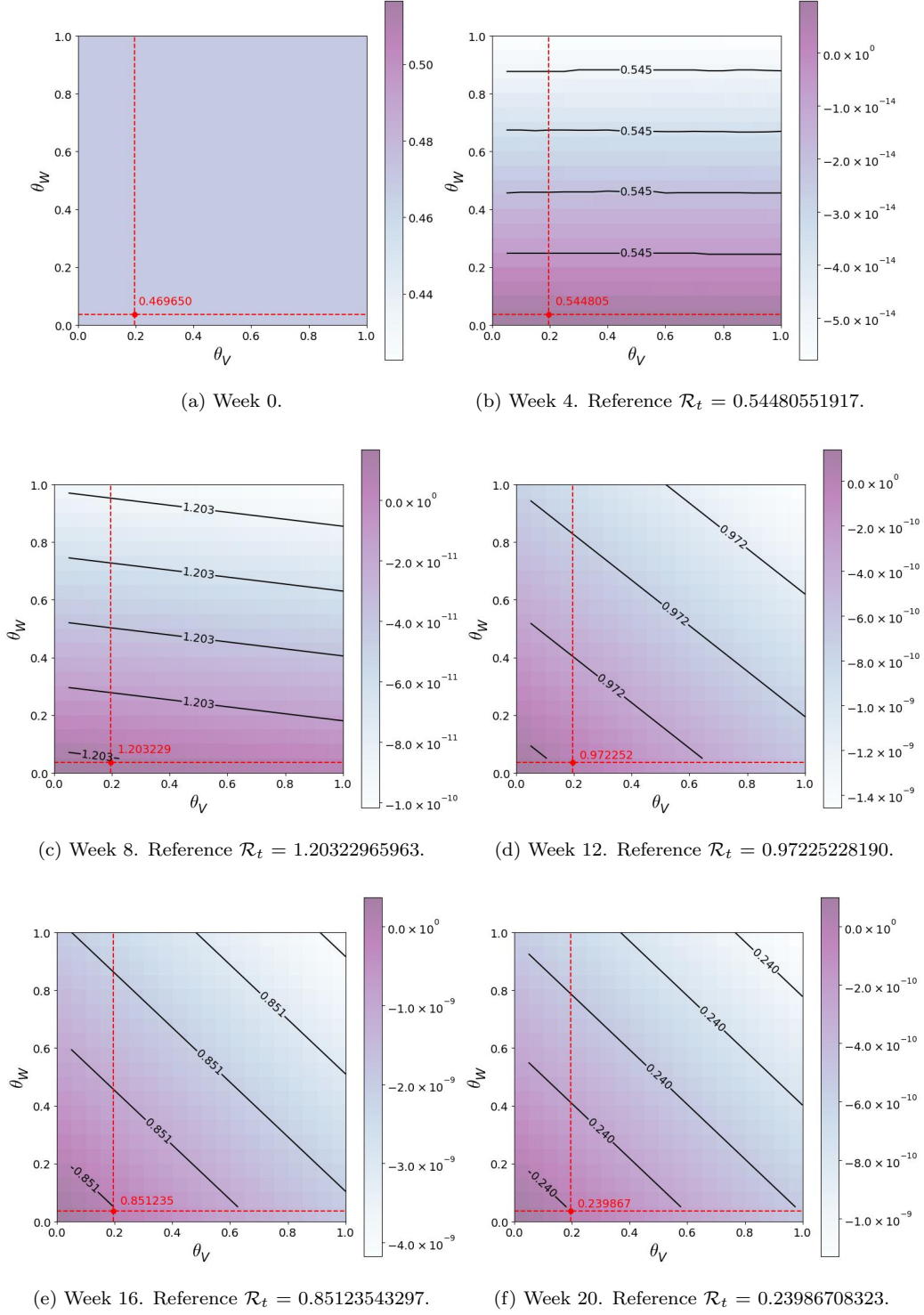
(f) Week 20. Reference $\mathcal{R}_t = 0.23986708323$.

Figure ST8: Reproduction number at different weeks depending on the value assigned to the effectivenesses of doses on severity. X-axis represents θ_V and Y-axis represents θ_W. The red point corresponds to the reference value, *i.e.* $\mathcal{R}_t$ value with θ_V, θ_W as in Table SF1. *Remark*: In Figures (b)-(f) the colorbar value stands for the increment or decrement with respect to the reference value.

136 S4. Validation results for the Inexact adjoint system

In this section we introduce some numerical tests corroborating the use of the inexact adjoint problem in the projected gradient algorithm described in section 2.3. We carried out some numerical experiments solving optimal control problems solving both the exact and inexact versions of the adjoint system for retrieving the multipliers associated to the descending gradient direction. We optimize the amount of doses to be distributed among the following three age classes:

$$N_A = \{(0 \div 19), (20 \div 39), (80+)\}.$$

137 Those age-classes are the ones that experience the greatest variations in terms of the number of vaccine admin-
138 istrations between the initial policy and the optimized policy for each cost functional (cfr. Section Results).
139 We solve the optimal control problems minimizing all cost functionals where the adjoint has been solved both
140 inexactly (blue policy) and exactly (green policy). We highlight that the delayed terms in the evolution equa-
141 tions of the Hamiltonian (whose order of magnitude is approximately 10 order of magnitude lower than the
142 other terms) are negligible:

$$\min_{t\in[0;T_f-t_a]} \left|\frac{\partial \mathcal{H}_X}{\partial S_i}(t)\right| \approx 10^{-3}, \quad \max_{t\in[t_a;T_f]} \left|\frac{\partial \mathcal{H}_X}{\partial Z_i}(t)\right| \approx 10^{-14}, \ \forall i \in N_A,$$

$$\min_{t\in[0;T_f-t_a]} \left|\frac{\partial \mathcal{H}_X}{\partial V_i}(t)\right| \approx 10^{-2}, \quad \max_{t\in[t_a;T_f]} \left|\frac{\partial \mathcal{H}_X}{\partial O_i}(t)\right| \approx 10^{-14}, \ \forall i \in N_A, \tag{3}$$

$$\min_{t\in[0;T_f-t_a]} \left|\frac{\partial \mathcal{H}_X}{\partial W_i}(t)\right| \approx 10^{-4}, \quad \max_{t\in[t_a;T_f]} \left|\frac{\partial \mathcal{H}_X}{\partial P_i}(t)\right| \approx 10^{-14}, \ \forall i \in N_A.$$

143 Therefore, the optimal policies, obtained employing the two different adjoint systems at each iteration step,
144 coincide (see Figures ST9–ST11). Actually, in each case we measured that

$$\max_{i\in N_A} ||\tilde{\mathbf{p}}_i - \mathbf{p}_i||_{2,t} \leq 10^{-10}, \tag{4}$$

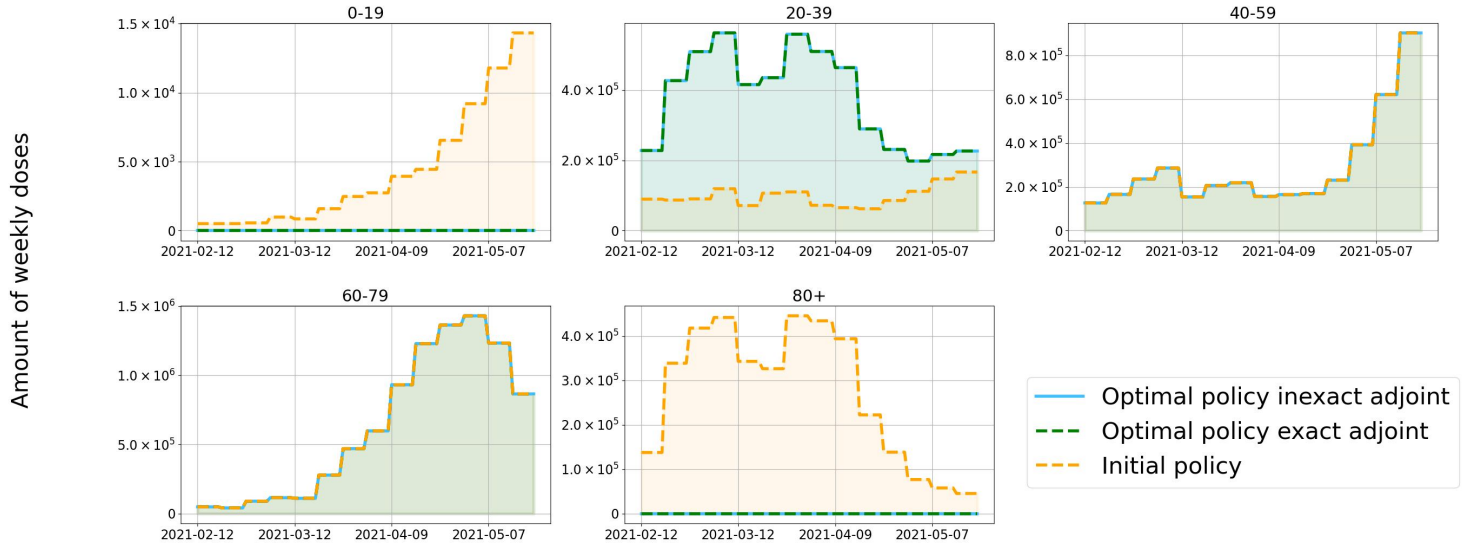145 adopting for $\tilde{\mathbf{p}}_i$ and $\mathbf{p}_i$ the same notation of Section 2.3.

Figure ST9: **Weekly amount of doses delivered for each age-stratification in the solutions minimizing infected starting from the Italian DPC policy and considering the three the exact and the inexact version of the adjoint system**.
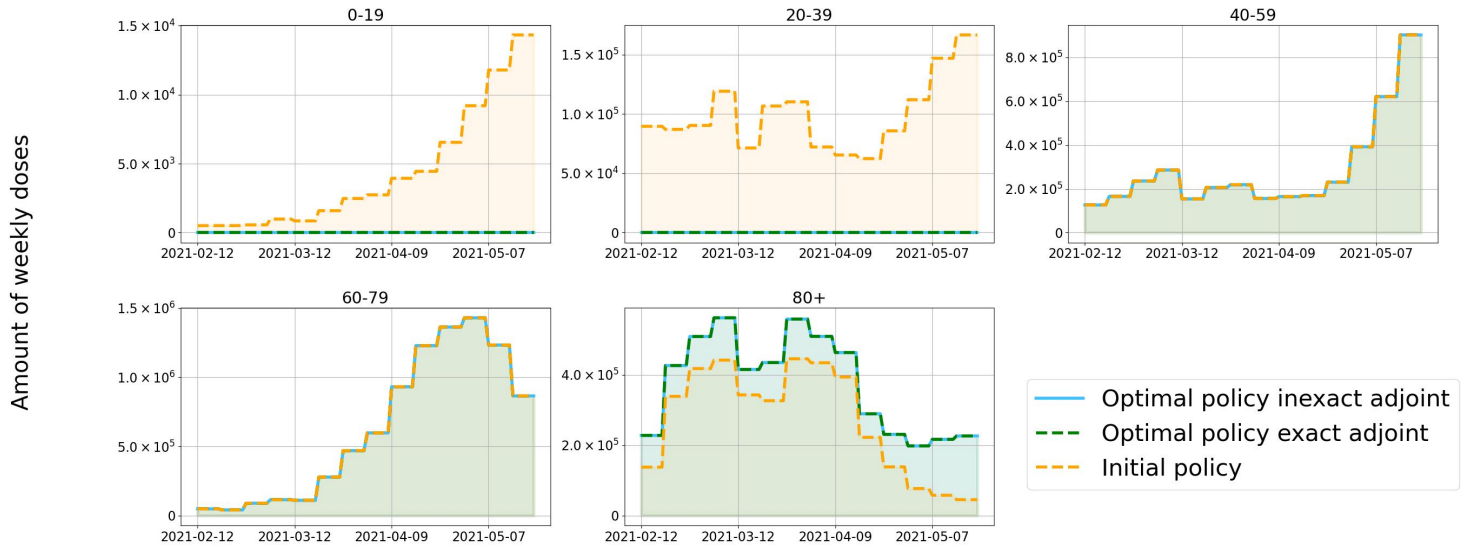

Figure ST10: **Weekly amount of doses delivered for each age-stratification in the solutions minimizing deceased starting from the Italian DPC policy and considering the three the exact and the inexact version of the adjoint system**.
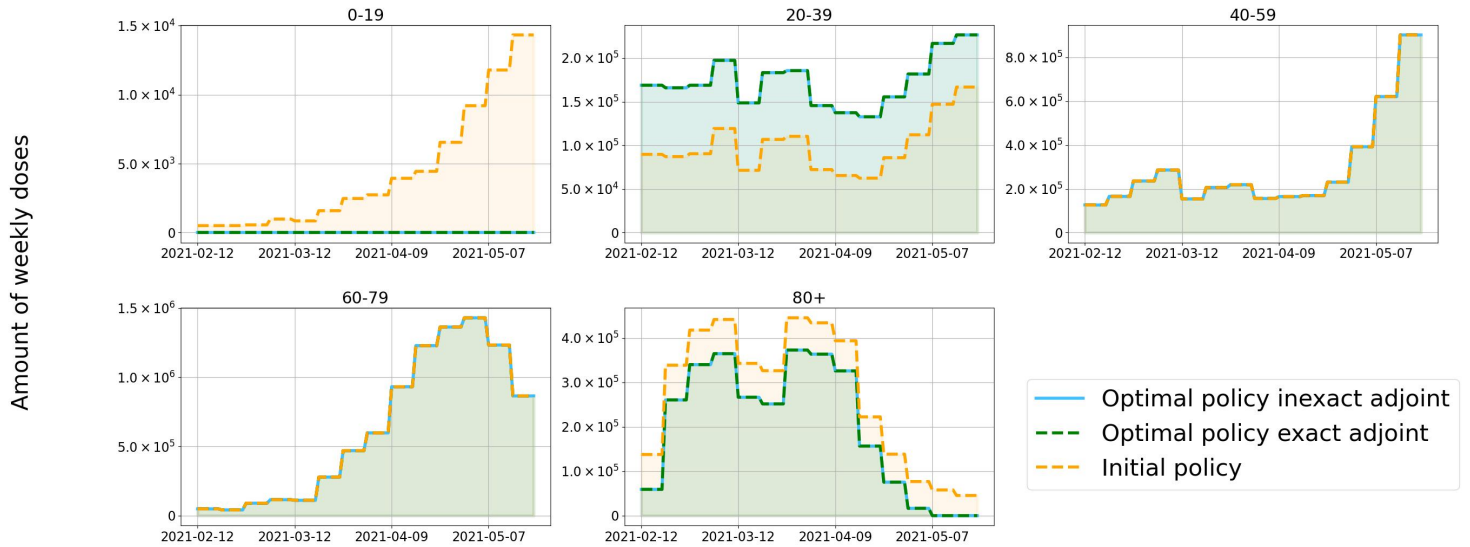
Figure ST11: **Weekly amount of doses delivered for each age-stratification in the solutions minimizing hospitalized starting from the Italian DPC policy and considering the three the exact and the inexact version of the adjoint system**.

146 References

1. Marziano V, Guzzetta G, Rondinone BM, Boccuni F, Riccardo F, Bella A, Poletti P, Trentini F, Pezzotti P, Brusaferro S, et al. Retrospective analysis of the Italian exit strategy from COVID-19 lockdown. Proceedings of the National Academy of Sciences 2021; 118

2. Parolini N, Dede' L, Antonietti PF, Ardenghi G, Manzoni A, Miglio E, Pugliese A, Verani M, and Quarteroni A. SUIHTER: A new mathematical model for COVID-19. Application to the analysis of the second epidemic outbreak in Italy. Proceedings of the Royal Society A 2021; 477:20210027

3. Mossong J, Hens N, Jit M, Beutels P, Auranen K, Mikolajczyk R, Massari M, Salmaso S, Tomba GS, Wallinga J, Heijne J, Sadkowska-Todys M, Rosinska M, and Edmunds WJ. Social Contacts and Mixing Patterns Relevant to the Spread of Infectious Diseases. PLOS Medicine 2008 Mar; 5:1–1. DOI: 10.1371/journal.pmed.0050074. Available from: https://doi.org/10.1371/journal.pmed.0050074

4. Zhang J, Litvinova M, Liang Y, Wang Y, Wang W, Zhao S, Wu Q, Merler S, Viboud C, Vespignani A, et al. Changes in contact patterns shape the dynamics of the COVID-19 outbreak in China. Science 2020; 368:1481–6

5. Voinsky I, Baristaite G, and Gurwitz D. Effects of age and sex on recovery from COVID-19: Analysis of 5769 Israeli patients. Journal of Infection 2020; 81:e102–e103

6. Hansen CH, Michlmayr D, Gubbels SM, Mølbak K, and Ethelberg S. Assessment of protection against reinfection with SARS-CoV-2 among 4 million PCR-tested individuals in Denmark in 2020: a population-level observational study. The lancet 2021; 397:1204–12

7. Lumley SF, O'Donnell D, Stoesser NE, Matthews PC, Howarth A, Hatch SB, Marsden BD, Cox S, James T, Warren F, et al. Antibody status and incidence of SARS-CoV-2 infection in health care workers. New England Journal of Medicine 2021; 384:533–40

8. Parolini N, Dede' L, Ardenghi G, and Quarteroni A. Modelling the COVID-19 epidemic and the vaccination campaign in Italy by the SUIHTER model. Infectious Disease Modelling 2022; 7:45–63

13

169   9.   Bernal JL, Andrews N, Gower C, Robertson C, Stowe J, Tessier E, Simmons R, Cottrell S, Roberts R, O'Doherty M, et al.
170   Effectiveness of the Pfizer-BioNTech and Oxford-AstraZeneca vaccines on covid-19 related symptoms, hospital admissions,
171   and mortality in older adults in England: test negative case-control study. bmj 2021; 373

172   10.   Tartof SY, Slezak JM, Fischer H, Hong V, Ackerson BK, Ranasinghe ON, Frankland TB, Ogun OA, Zamparo JM, Gray S,
173   et al. Effectiveness of mRNA BNT162b2 COVID-19 vaccine up to 6 months in a large integrated health system in the USA:
174   a retrospective cohort study. The Lancet 2021; 398:1407–16

175   11.   Presidenza del Consiglio dei Ministri, Dipartimento della Protezione Civile, Italia. Database. Available from: `https://github.`
176   `com/italia/covid19-opendata-vaccini`

177   12.   Presidenza del Consiglio dei Ministri, Dipartimento della Protezione Civile, Italia. Database. Available from: `https://github.`
178   `com/pcm-dpc/COVID-19`

179   13.   Comunian A, Gaburro R, and Giudici M. Inversion of a SIR-based model: A critical analysis about the application to
180   COVID-19 epidemic. Physica D: Nonlinear Phenomena 2020; 413:132674

181   14.   Dantas E, Tosin M, and Cunha Jr A. Calibration of a SEIR–SEI epidemic model to describe the Zika virus outbreak in Brazil.
182   Applied Mathematics and Computation 2018; 338:249–59

183   15.   Marinov TT and Marinova RS. Dynamics of COVID-19 using inverse problem for coefficient identification in SIR epidemic
184   models. Chaos, Solitons & Fractals: X 2020; 5:100041

185   16.   Marinov TT, Marinova RS, Omojola J, and Jackson M. Inverse problem for coefficient identification in SIR epidemic models.
186   Computers & Mathematics with Applications 2014; 67:2218–27

187   17.   Daza-Torres ML, Capistrán MA, Capella A, and Christen JA. Bayesian sequential data assimilation for COVID-19 forecasting.
188   Epidemics 2022; 39:100564

189   18.   Xu J and Tang Y. Bayesian framework for multi-wave COVID-19 epidemic analysis using empirical vaccination data. Math-
190   ematics 2021; 10:21

191   19.   Korostil IA, Peters GW, Cornebise J, and Regan DG. Adaptive Markov chain Monte Carlo forward projection for statistical
192   analysis in epidemic modelling of human papillomavirus. Statistics in medicine 2013; 32:1917–53

193   20.   Wieczorek M, Siłka J, and Woźniak M. Neural network powered COVID-19 spread forecasting model. Chaos, Solitons &
194   Fractals 2020; 140:110203

195   21.   Zisad SN, Hossain MS, Hossain MS, and Andersson K. An integrated neural network and SEIR model to predict Covid-19.
196   Algorithms 2021; 14:94

197   22.   Li M, Zhang Z, Jiang S, Liu Q, Chen C, Zhang Y, and Wang X. Predicting the epidemic trend of COVID-19 in China and
198   across the world using the machine learning approach. medRxiv 2020

199   23.   Nabi KN, Tahmid MT, Rafi A, Kader ME, and Haider MA. Forecasting COVID-19 cases: A comparative analysis between
200   recurrent and convolutional neural networks. Results in Physics 2021; 24:104137

201   24.   Mohimont L, Chemchem A, Alin F, Krajecki M, and Steffenel LA. Convolutional neural networks and temporal CNNs for
202   COVID-19 forecasting in France. Applied Intelligence 2021; 51:8784–809

203   25.   Rasmussen DA, Ratmann O, and Koelle K. Inference for nonlinear epidemiological models using genealogies and time series.
204   PLoS computational biology 2011; 7:e1002136

205   26.   Diekmann O, Heesterbeek J, and Roberts MG. The construction of next-generation matrices for compartmental epidemic
206   models. Journal of the royal society interface 2010; 7:873–85